Time and Space Spectral Analyses of Southern Hemisphere Sea Level Pressure Variability

DAVID A. JONES AND IAN SIMMONDS

Department of Meteorology, University of Melbourne, Parkville, Victoria, Australia

(Manuscript received 24 April 1992, in final form 10 July 1992)

ABSTRACT

This study examines the time–space structure of the standard deviation of daily summer and winter mean sea level pressure over the Southern Hemisphere, as identified in 20 years of analyses generated by the Australian Bureau of Meteorology and two long simulations with a GCM. The unfiltered variability derived from the operational analyses generally display a deal of zonal symmetry, particularly during the summer period, with maxima in the midlatitudes. The percentage of the temporal variance which is explained by the bandpass and low-pass components is calculated; in January and July the percentage of the variance explained by the bandpass data is maximized between 30° and 60°S and assumes values of typically 25%. In general, the low-pass data account for more of the variance and tends to achieve its maxima in low and high latitudes. The greatest contribution to the low-frequency field comes from the planetary-scale waves, particularly at higher latitudes. The synoptic and small-scale waves are generally found to be the dominant contributors to the variance in the higher-frequency bandpass fields, particularly in the region of the hemispheric storm track.

Similar analyses applied to the output of the GCM suggest that, overall, the model performs reasonably well, although the quality of the simulation of the low-frequency variability is inferior to that of the synoptic time scales. The tendency of the model to overpredict the winter daily mean sea level pressure variability in the South Pacific appears to be mostly due to this error in the low-frequency part of the field.

These results reveal a considerable difference between the location of cyclone centers and bandpassed mean sea level pressure variability in the high southern latitudes. The model data imply that the maxima of the bandpassed variability tend to be some 30°–40° of longitude to the west and 5°–7° latitude to the north of those of cyclone centers. This serves to underline the dangers and ambiguity of referring to regions of high variability as "storm tracks."

1. Introduction

Due to a paucity of data and other problems, the study of the modes of variability over the Southern Hemisphere (SH) has received comparatively little attention. However, the understanding of the general behavior of atmospheric transients can be illuminated by their structure and governing mechanisms in that hemisphere. The very different distributions of continents and topography in the two hemispheres are known to be important in giving rise to distinct mean patterns of atmospheric variables. Similar processes are also obviously at work in the determination of the temporal and spatial behavior of transient disturbances (including storms and their characteristic tracks), although the mechanisms are more subtle. Hoskins and Valdes (1990) suggested that the crucial ingredient in the existence of mean conditions suitable for the existence of the two Northern Hemisphere (NH) storm tracks is the mean diabatic heating in the region of the tracks, off the east coast of the continents. They point out that the geography in the south is very different and that the extended, but less definite, storm track in the SH could be rather different in its maintenance.

An important reason for studying variability is its association with regions of storms and extreme weather. Also, in terms of the large scale, it allows that the role played by transient disturbances in maintaining the various atmospheric budgets to be identified. This latter justification is all the more relevant in the SH extratropics where, for example, the transient disturbances play a much greater role in transporting heat poleward than they do in the Northern Hemisphere (e.g., Trenberth 1981). In addition, the study of observed atmospheric variability is of importance in that it provides criteria against which the output of general circulation models (GCMs) can be assessed.

Given the aforementioned difficulties with data paucity and veracity, it is not surprising that there have only been a handful of studies devoted to short-period variability in the SH. The most important of these include Trenberth (1981, 1991), Physick (1981), Oort

Corresponding author address: Ian Simmonds, Department of Meteorology, University of Melbourne, Parkville, Victoria, Australia, 3052.

(1983), Kep (1984), James and Anderson (1984), Le Marshall et al. (1985), and Simmonds et al. (1990) (hereafter referred to as SIM).

In this paper we present the day-to-day variability of summer and winter mean sea level pressure (MSLP) calculated over the SH from the Australian Bureau of Meteorology's SH hemispheric analyses (denoted as the ASH) set and from two long GCM climate simulations. The length of the ASH data series used here (July 1972–July 1991) is the longest considered in any study of this sort (and includes the most recent and reliable data) and, as such, the results must be considered as the most representative. The variability that survives bandpass and low-pass filters for the two data sources will then be computed. We also examine the spatial scales that are associated with the various transient features.

We have purposely focused this study on the modes of variation of the mean sea level pressure because of its intimate association with surface weather and are particularly interested in the mid and high southern latitudes. We also interpret some of our results in terms of the ambiguity surrounding the term *storm tracks*. The variability that remains after the daily data have been subject to the high-pass filter can be compared to previously published statistics on the distribution of low pressure centers in the SH.

2. Datasets and methods

The observational analyses used here are a subset of the twice-daily dataset of the Melbourne World Meteorological Centre's operational hemispheric analyses. These analyses are available on a 47 × 47 polar stereographic grid over the Southern Hemisphere, giving an effective resolution of typically 500 km (Guymer 1986). This hemispheric dataset has been used in a number of previous SH studies, including those of Swanson and Trenberth (1981), Trenberth (1981), Le Marshall et al. (1985), Karoly and Oort (1987), and SIM. The quality of the data has been discussed by these authors. Some have pointed out discrepancies between the 1100 and 2300 UTC analyses, and the 2300 UTC analyses were considered superior. It is the latter we use in the present study.

We have extracted the once-daily MSLP analyses for the months of January and July. Nineteen years (1973–91) were obtained for January and 20 (1972–91) for July. Periods with missing data were filled by a temporal linear interpolation using data values at the times closest to the observing time for which the data were missing. (During the entire period, only 10 days were missing for winter and 11 for summer.) The hemispheric analyses gridded on the polar stereographic grid were then interpolated onto a 5° × 5° latitude–longitude grid covering the SH.

We also perform time–space analyses on a dataset generated in a January and a July "perpetual-month" 600-day GCM simulation. (The sets are identical to those analyzed in SIM.) The model used is the rhomboidal 21-wavenumber version of the Melbourne University GCM (Simmonds 1985; Simmonds et al. 1988). We mention that the version of the model used here contains no temporal variations in the boundary conditions, such as those resulting from fluctuations in sea surface temperature, ozone, cloud amounts, or insolation. The effect of fixed external boundary conditions will be alluded to later.

The transient structure of the atmosphere as inferred from the two datasets has been investigated through a combined temporal–spatial spectral analysis. The technique used is to calculate the temporal standard deviation at each point after the data have been subject to various combinations of filtering.

A temporal breakdown of the fields has been achieved through the use of two time filters, a low-pass filter active for variations of 10 or more days, and a bandpass filter active in the period band 2.5–6 days. The time filters are those defined by Blackmon and Lau (1980) and have the form

$$\tilde{f}_j = a_0 f_j + \sum_{k=1}^{10} a_k [f_{j+k} + f_{j-k}], \qquad (1)$$

where f_j is the unfiltered data at day j, $\tilde{f}_j$ its filtered counterpart, and the a_k are the filter coefficients. The values to which these coefficients are set (the same used by Blackmon and Lau) give rise to the low-pass and bandpass filters whose frequency responses are shown in Fig. 1.

The scale breakup of the spatial distribution of the MSLP is performed in terms of spherical harmonic analysis and follows the scale separation proposed by Blackmon (1976). In this, the distribution of a 2D variable f is approximated by the form

$$f(\lambda, \theta) = \sum_{m=-M}^{M} \sum_{n=|m|}^{|m|+M} f_{m,n} Y_{m,n}(\lambda, \theta), \qquad (2)$$

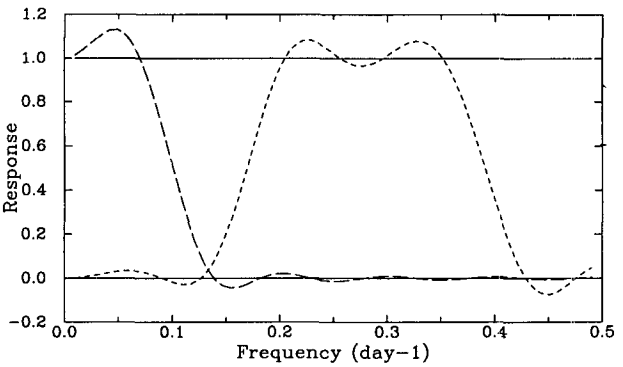

FIG. 1. The frequency responses of the bandpass (short dash) and low-pass (long dash) time filters.

where $f_{m,n}$ are (complex) coefficients, $Y_{m,n}(\lambda, \theta)$ is the spherical harmonic of order m and degree n, and M is the truncation wavenumber.

In this paper we confine ourselves to three scales or regimes. These are

regime I: $0 \leqslant n \leqslant 6$

regime II: $7 \leqslant n \leqslant 12$

regime III: $13 \leqslant n \leqslant 18$.

We refer to these regimes as long (or planetary) waves, medium (or synoptic) waves, and short waves, respectively.

3. Application of the analysis techniques

In studies in which comparisons are to be made between observational analyses and simulated data generated from a "perpetual-month" climatic simulation, the question of the removal of the seasonal cycle in the observational data arises. A related but separate question is how one defines climatologies of statistics based on deviations from the average for a given month of the year when, of course, the months do not constitute a continuous time series.

In this paper, the statistics are calculated using the "separate-month" method. This involves calculating the variability in each individual month in the dataset and then determining the means of these over the required time period. It is known that this technique underestimates the standard deviation calculated from a long perpetual-month simulation by about 10% (SIM) but has the advantage of being applicable to the observed analyses. The application of the time filters (1) poses the question as to how to deal with the "boundaries" of the months. We have performed unbiased filtering as follows. With the ASH set we have taken the data from 10 days before the start of the month to 10 days after the end of it (e.g., 22 December–10 February for the January case). The filtered data were then obtained for the 31 days of the Januarys and Julys, and the standard deviation of these was determined. In the case of the GCM output, the variability in each of the twenty 30-day months was calculated for both seasons, the filter being applied to the data, including the previous and subsequent 10 days of data.

4. Temporal-filtered variability

a. Variability in the Southern Hemisphere analyses

In this section, the regional characteristics of the transient structure, as inferred by the ASH analysis set, are presented. Figure 2a shows the geographical distribution of the unfiltered standard deviation for the January MSLP corresponding to the untruncated, unfiltered field. The plot displays a considerable degree of zonal symmetry with maxima near 55°S. However, near this belt a three-wave pattern is evident. The principal maximum is located in the New Zealand sector, a finding in agreement with that of Trenberth (1981). This region has been well documented as a favored location for the development of strong, equivalent barotropic slow-moving anticyclones (blocks) (van Loon 1956; Taljaard 1972; Trenberth 1975; Trenberth and Mo 1985), which are associated with a local enhancement of the climatological split in the mean westerlies. The other maxima are located in the south Indian Ocean and to the east of the Drake Passage.

We have computed the variability that remains after the data have been subject to the bandpass and low-pass filters described earlier. Ideally, we could have shown similar plots of these quantities but, in the interest of brevity, we have decided to show only the percentage of the variance exhibited in the unfiltered data due to the two filters. This novel presentation allows an immediate appreciation of the geographical distribution of the contributions to the total variance. Shown is the ratio of the squares of the temporal standard deviations of the filtered and unfiltered data, the result being multiplied by 100 in order to be expressed as a percentage of explained variance. [We have stippled those regions where the percentage of variance exceeds 60% and 80% (heavy stippling) and hatched those over which the relevant filter explains less than 10%.] The percentage explained by the bandpass data reaches maxima between 30° and 60°S (Fig. 2b), with spot values only just exceeding 40%. The bandpass data account for only about one-quarter of the total variability. The amount explained in the low-pass component (Fig. 2c) is, in general, greater and assumes its largest values equatorward of 30°S, particularly in the west Pacific and in the high southern latitudes.

Similar displays are presented for July in Fig. 3. The temporal variability of the unfiltered field [part (a)] shows a broad band of large variability from middle to high latitudes. The tropics and polar regions are characterized by smaller values with the hemispheric maxima in the variability generally located to the southeast of the three nonpolar continents, regions noted previously to be the favored locations for the existence of blocking anticyclones. Overall, the variability in July is considerably enhanced over that exhibited in the summer. A plot of the difference between the winter and summer variability (not shown) reveals that the greatest enhancements tend to occur near 40°S, with local maxima just to the west of the three continents. The greatest increase in the winter is in excess of 5 hPa and occurs near the Larsen Ice Shelf. The geographical distribution of the variance explained by the bandpassed data (Fig. 3b) bears some resemblance to that in January, except the values are somewhat smaller. There is also some similarity for the low-pass data in the two months, particularly between 90° and 270°E; both months exhibit relatively small amounts of variance explained to the south and southwest of Australia, high values over a large region centered on

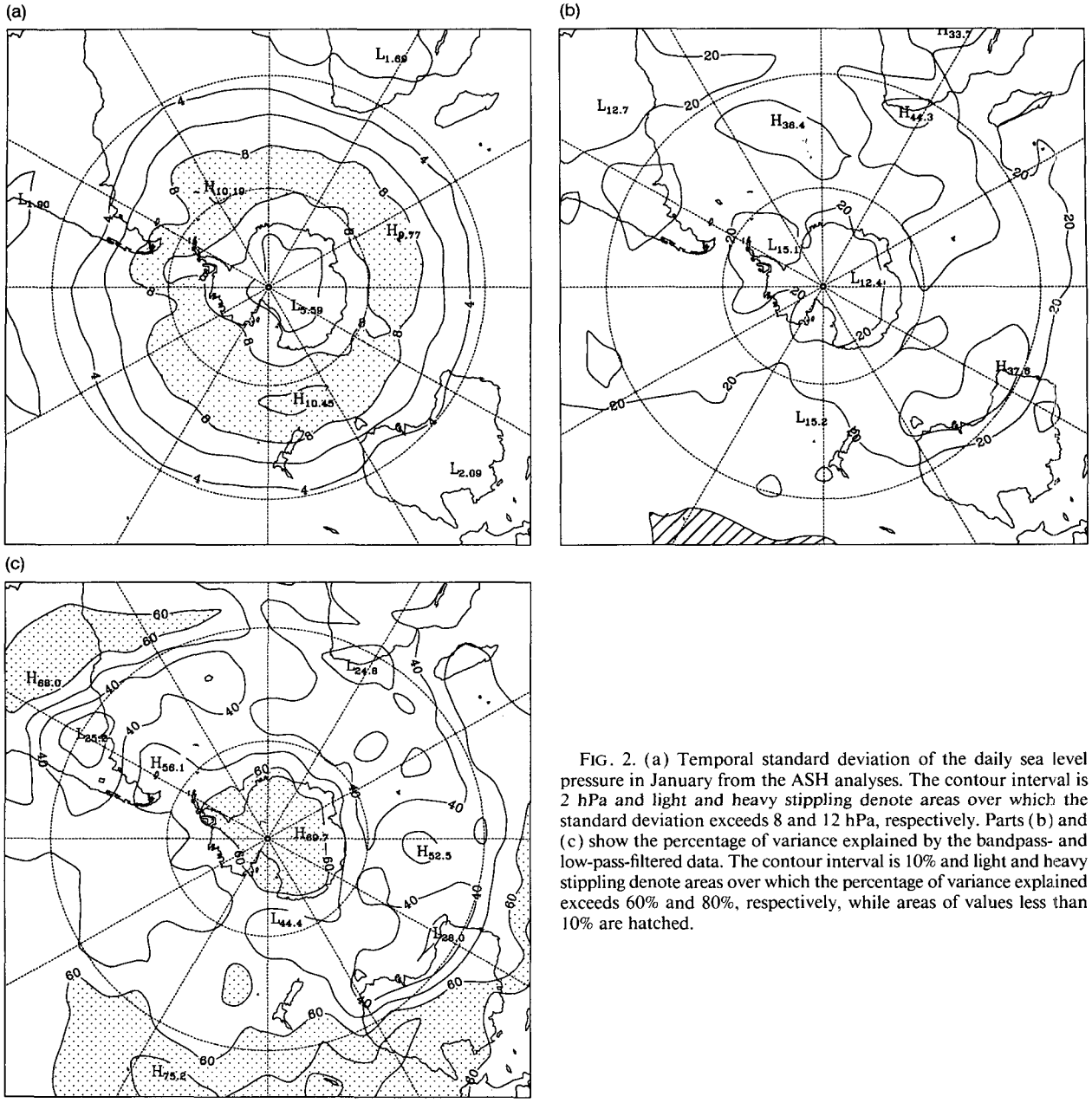

FIG. 2. (a) Temporal standard deviation of the daily sea level pressure in January from the ASH analyses. The contour interval is 2 hPa and light and heavy stippling denote areas over which the standard deviation exceeds 8 and 12 hPa, respectively. Parts (b) and (c) show the percentage of variance explained by the bandpass- and low-pass-filtered data. The contour interval is 10% and light and heavy stippling denote areas over which the percentage of variance explained exceeds 60% and 80%, respectively, while areas of values less than 10% are hatched.

New Zealand (a region of preferred blocking activity), and low values to the west of South America.

b. *Simulated variability*

We next display the above aspects of variability as simulated in our two perpetual-month model runs. The distribution of the temporal standard deviation of the unfiltered MSLP for the January case is shown in Fig. 4a. Comparison with Fig. 2a suggests that the model has captured the structure fairly well. In SIM we had remarked that the model appears to overpredict slightly the level of variability, when comparison was made with the atlas of Oort (1983). A similar statement appears to be true when comparison is made with this long ASH set, particularly in the east Pacific near 60°S. However, comparison of Fig. 2a and Fig. 1b in SIM shows considerable differences between these two observed datasets, especially to the south of New Zealand and over a region centered on the Drake Passage.

The percentage of variance in the bandpass data achieves maxima around the 40°S latitude (Fig. 4b). The numerical values are similar to those in the observed set, and there is a suggestion of ridges of high variance, explained as extending east-southeast across the Atlantic and Indian oceans, similar to the observed.

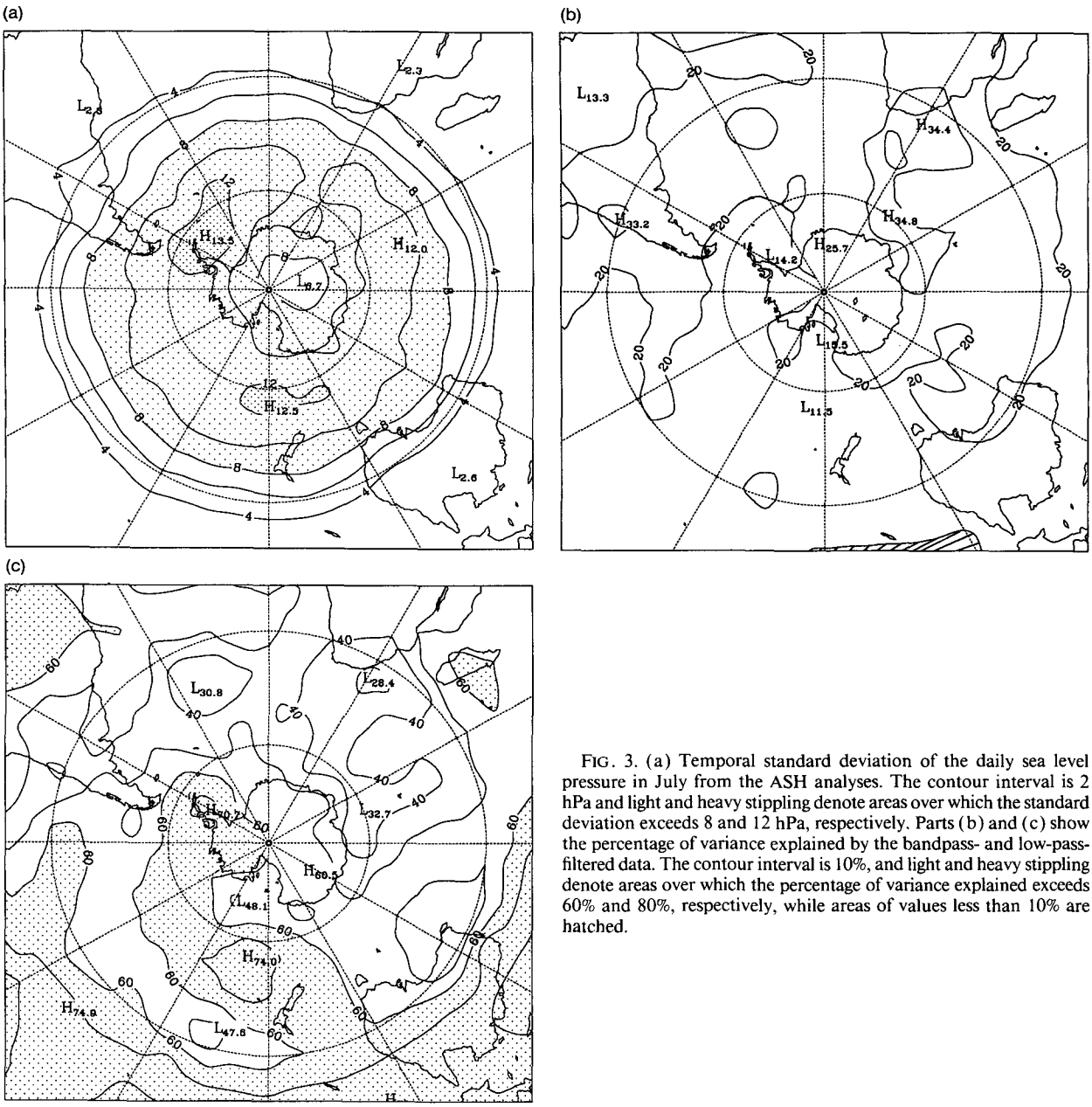

FIG. 3. (a) Temporal standard deviation of the daily sea level pressure in July from the ASH analyses. The contour interval is 2 hPa and light and heavy stippling denote areas over which the standard deviation exceeds 8 and 12 hPa, respectively. Parts (b) and (c) show the percentage of variance explained by the bandpass- and low-pass-filtered data. The contour interval is 10%, and light and heavy stippling denote areas over which the percentage of variance explained exceeds 60% and 80%, respectively, while areas of values less than 10% are hatched.

The low-pass data (Fig. 4c) explains most of the variance at high and low latitudes, particularly over ocean areas, which is in agreement with the analyses based on the ASH dataset.

The modeled distributions of variability in July are shown in Fig. 5. The unfiltered data exhibit [part (a)] a low-latitude minimum, a belt of large variability in the midlatitudes, and a relative minimum over the Antarctic continent. The belt of large variability shows little latitudinal shift relative to the January simulation, a finding also apparent in the observations (Figs. 2a and 3a). This absence of substantial seasonality in the latitudinal position of the band of maximum variability has been noted previously in the studies of Kao et al. (1970), Jenne et al. (1974), Oort (1983), Le Marshall et al. (1985), and Trenberth (1991). The field throughout the Pacific is dominated by a spurious maximum, upstream of the Drake Passage. Throughout the mid and high latitudes, the model simulates greater values than the ASH statistics, this being most marked in the Pacific region. The tropics in contrast show a general underestimate of the observed variability, a finding noted previously in the January statistics; this suggests the substantial part that forced variations play in the total variability of the atmosphere throughout the tropics.

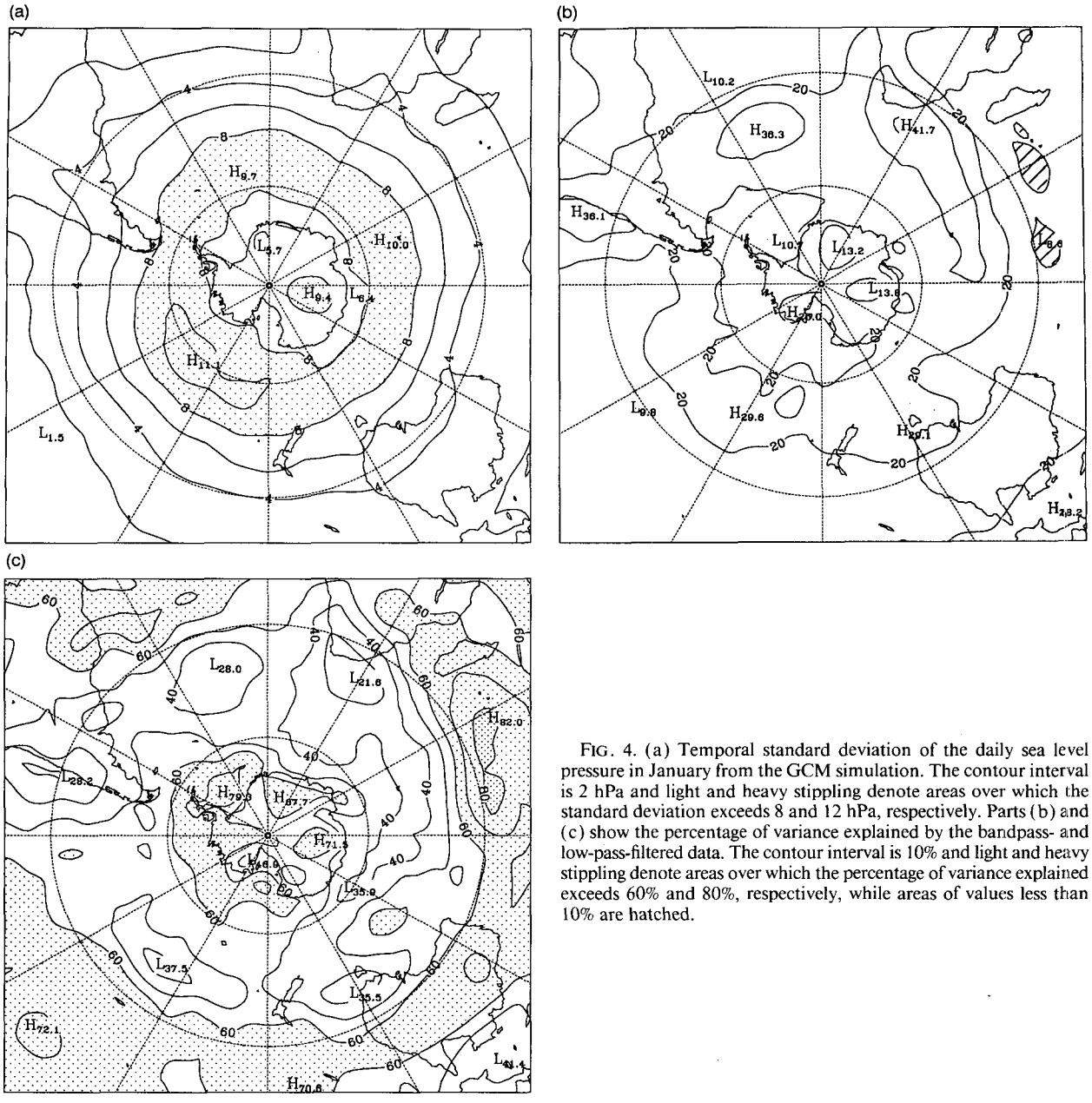

FIG. 4. (a) Temporal standard deviation of the daily sea level pressure in January from the GCM simulation. The contour interval is 2 hPa and light and heavy stippling denote areas over which the standard deviation exceeds 8 and 12 hPa, respectively. Parts (b) and (c) show the percentage of variance explained by the bandpass- and low-pass-filtered data. The contour interval is 10% and light and heavy stippling denote areas over which the percentage of variance explained exceeds 60% and 80%, respectively, while areas of values less than 10% are hatched.

The percentage of variance explained by the model bandpassed data is shown in Fig. 5b. As for the observations, typically only about 20% of the variance is explained by oscillations in this temporal band, with values reaching as low as less than 10% and almost 40%. As in January, the variance explained by the slower modes (Fig. 5c) is, for the most part, much greater. The pattern has features similar to those found in the observations (Fig. 3c), including relatively low values over the southern parts of the three continents and high values around the coast of Antarctica and its interior. The large simulated value near the Bellingshausen Sea indicates that the spuriously large variability of the unfiltered data is due predominantly to long-period oscillations in this region.

5. Zonal averages

Next we explore the contribution of various time and spatial scales to the temporal variability of the real and modeled atmospheres. This is presented in the form of zonal averages of standard deviations calculated after the application of various time and space filters. The presentation of these is a convenient summary, and the SH lends itself, to some extent, to be described in terms of zonal averages, partly because

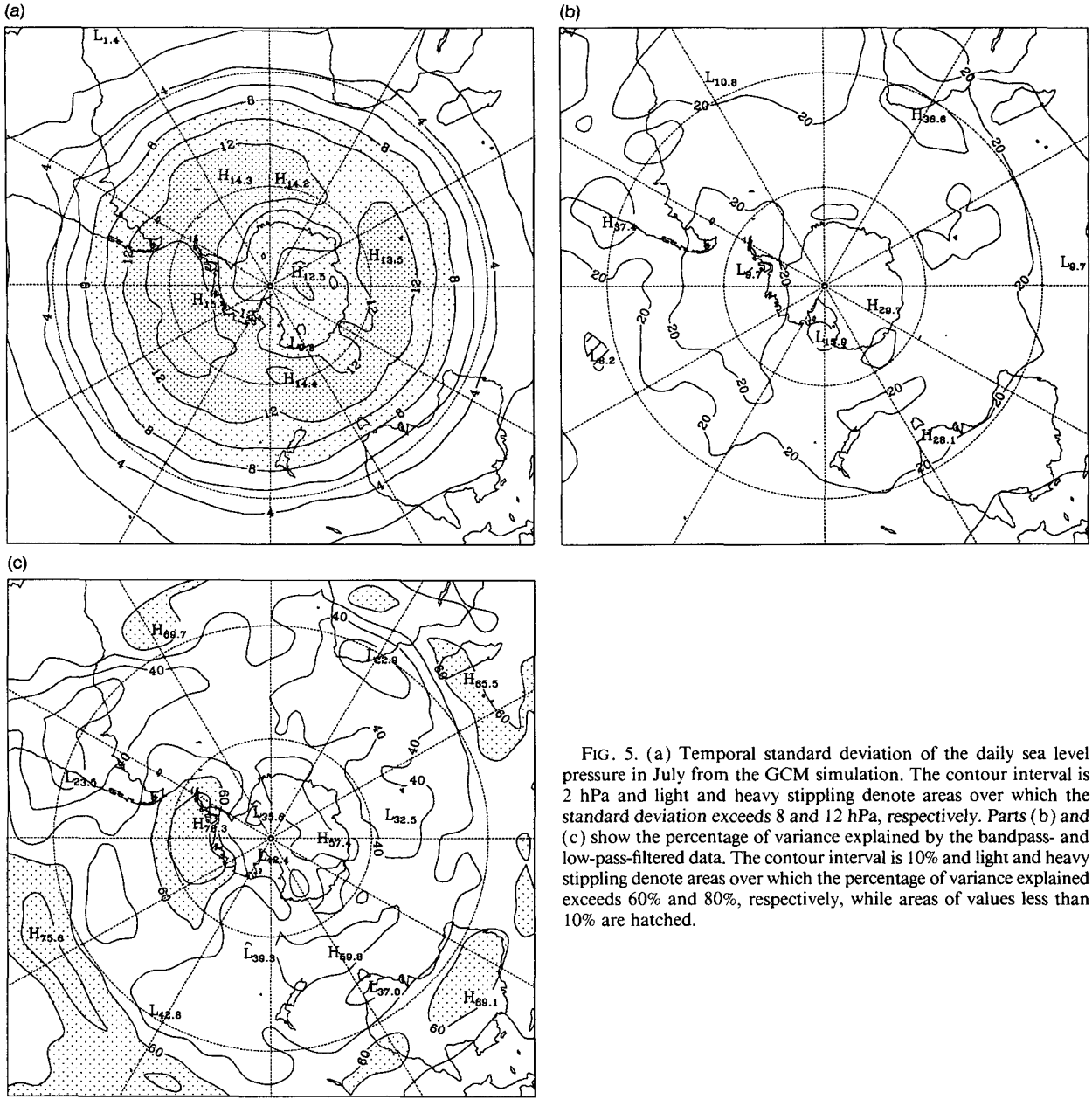

FIG. 5. (a) Temporal standard deviation of the daily sea level pressure in July from the GCM simulation. The contour interval is 2 hPa and light and heavy stippling denote areas over which the standard deviation exceeds 8 and 12 hPa, respectively. Parts (b) and (c) show the percentage of variance explained by the bandpass- and low-pass-filtered data. The contour interval is 10% and light and heavy stippling denote areas over which the percentage of variance explained exceeds 60% and 80%, respectively, while areas of values less than 10% are hatched.

variability and storm tracks are not dominated by jet stream entrance and exit regions (Trenberth 1991). Figure 6 presents the zonal average of the observed January variability associated with the spatially unfiltered fields (TOT) and with regimes I, II, and III for the temporally unfiltered data [part (a)], the bandpass data [part (b)], and the low-pass data [part (c)]. In Fig. 6a the total variability is seen to peak at in excess of 8 hPa at about 55°S. The variability associated with the long waves (regime I) increases almost monotonically with latitude and assumes values in excess of 5 hPa near the Antarctic coast. (This quasi-monotonic behavior is typical of all the plots shown here for summer and winter for both the observations and the model simulations.) The peak of the regime II data is achieved some 5° equatorward of that of the total, and the deviation accounted for by the short waves (regime III) is typically 2 hPa. The zonally averaged variation on the bandpass data for these space domains (Fig. 6b) shows rather similar patterns but with magnitudes typically half of those exhibited by the temporally unfiltered data. The low-pass variability associated with TOT, regime I, and regime II spatial bands, shown in Fig. 6c, are greater than those in the bandpass data.

A similar presentation for the July observed data is made in Fig. 7. All the remarks made above are applicable to the July case, except the magnitude of the variability tends to be somewhat greater in the winter

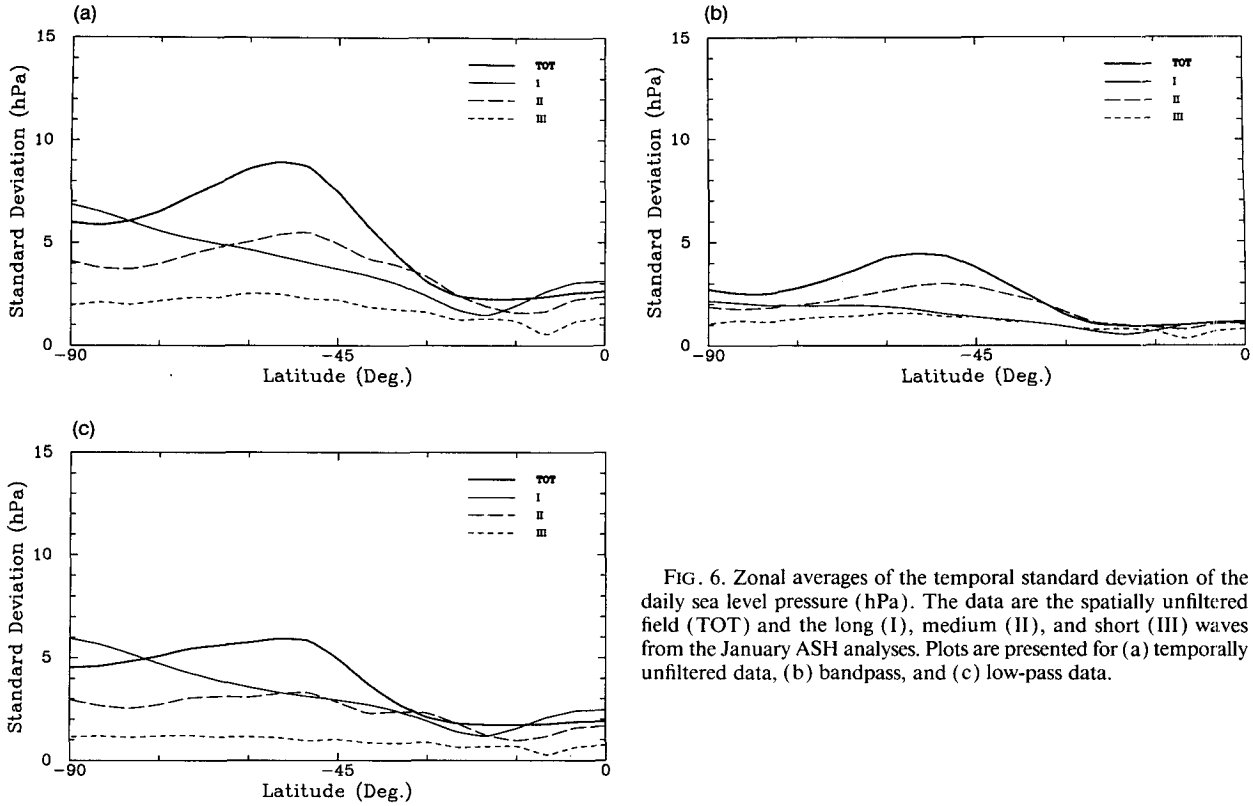

FIG. 6. Zonal averages of the temporal standard deviation of the daily sea level pressure (hPa). The data are the spatially unfiltered field (TOT) and the long (I), medium (II), and short (III) waves from the January ASH analyses. Plots are presented for (a) temporally unfiltered data, (b) bandpass, and (c) low-pass data.

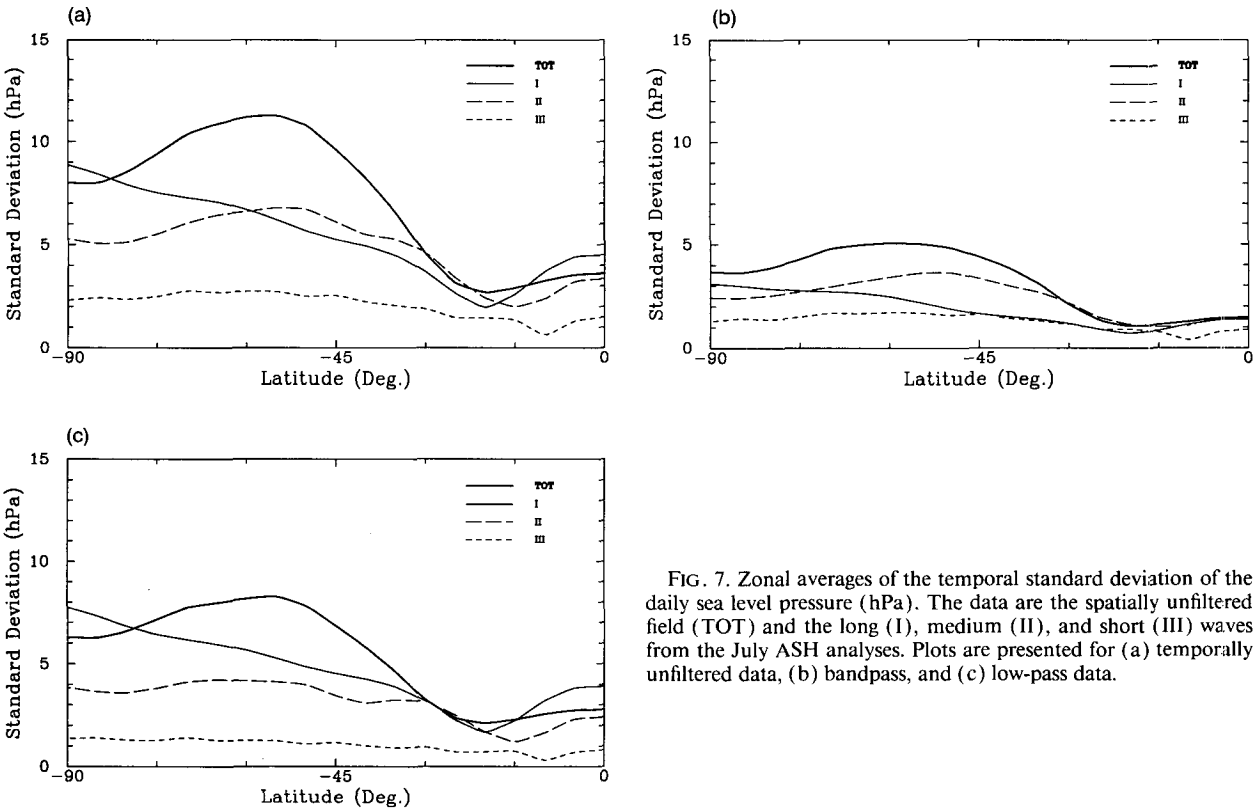

FIG. 7. Zonal averages of the temporal standard deviation of the daily sea level pressure (hPa). The data are the spatially unfiltered field (TOT) and the long (I), medium (II), and short (III) waves from the July ASH analyses. Plots are presented for (a) temporally unfiltered data, (b) bandpass, and (c) low-pass data.

month. (For example, the maximum of the unfiltered variability is in excess of 11 hPa.) There is no clear shift in the latitudes of the various maxima between the seasons.

The comparable statistics as simulated by the GCM are shown in Figs. 8 and 9 for January and July, respectively. In general, the agreement with the observed data in January is rather good. Points of divergence include a tendency of the model to overestimate the total variability (associated with the low-pass part of the signal) and that in the model the variability in the temporally unfiltered data peaks at about the same latitude in both the TOT and regime I data. The model also shows enhanced variability associated with the short waves (regime III); it is not clear whether this is associated with the accuracy of the treatment of these waves in the model or their representation in the ASH analyses.

The agreement with observations is not as good in July. The maximum for the unfiltered data (Fig. 9a) is about 3 hPa greater than, and some 5° south of, that observed. The variability associated with the long waves appears to be well captured, but there is too much in the medium and short waves. Much of the error in the simulation can be attributed to the behavior of the low-frequency modes; the model simulation of the contributions made by the band-filtered data (Fig. 9b) appear reasonably in accord with the observations, while, for example, the maximum of the low-frequency TOT field (Fig. 9c) occurs more than 10° too far south and is some 3 hPa too strong.

6. Variability and storm tracks

An important reason for studying variability is its association with regions of storm tracks and extreme weather. Trenberth (1981) has pointed out that from a synoptic viewpoint, storm tracks cannot be unambiguously defined. This caution has been raised by many authors, including Wallace et al. (1988) and Hoskins and Valdes (1990). Many authors have regarded storm tracks as synonymous with the maxima of the high-frequency height variability. This definition has the advantage of being objective and easily calculated, but it is not entirely clear how the principal axes of this quantity relate to other measures or definitions of storm tracks. Alternative measures used in the SH include the frequency of surface fronts and of low centers (van Loon 1965; Kep 1984), cloud signatures from satellite pictures (Carleton 1979), the evaluation of the high-pass velocity correlation tensor (Hoskins et al. 1983), baroclinic waveguides (Wallace et al. 1988), and a range of eddy quantities [e.g., James and Anderson (1984) used transient kinetic energy]. Trenberth (1986, 1991) has elegantly shown the relationship between a number of these measures and has clarified the reasons for important differences in the latitude of their maxima.

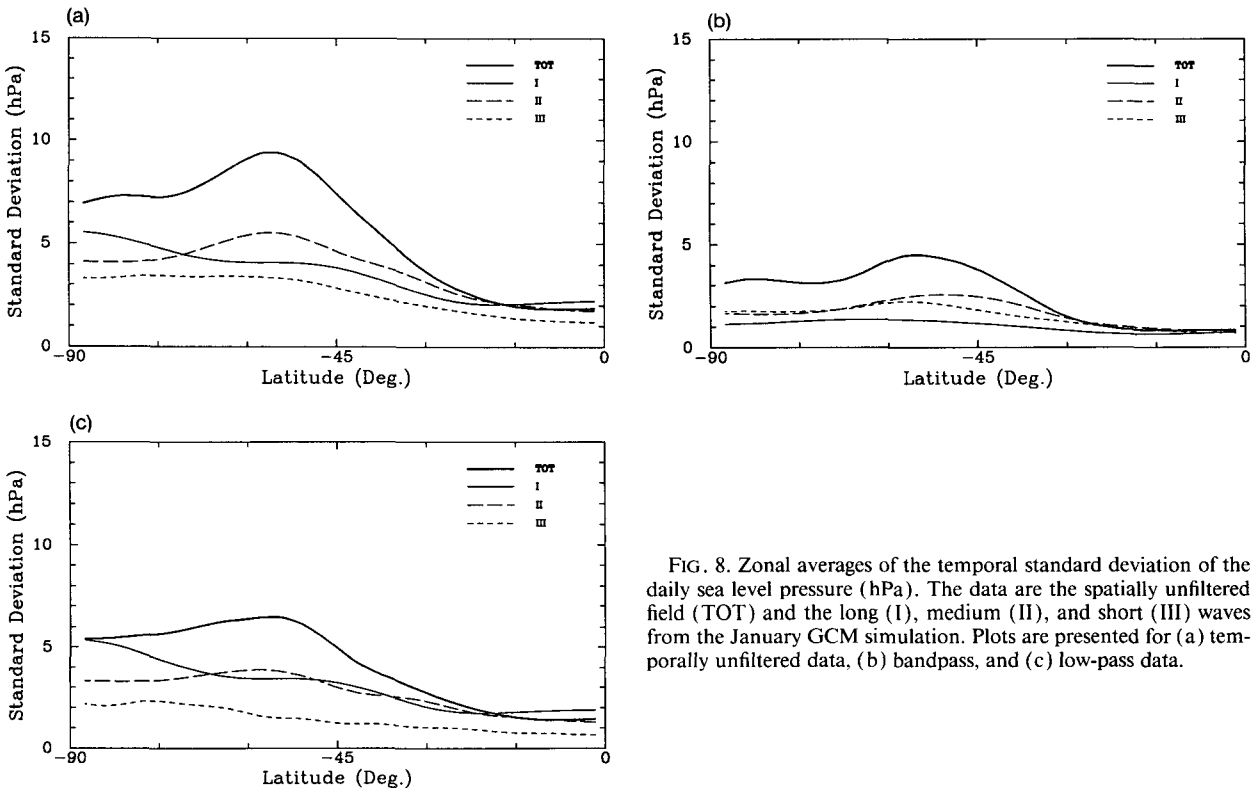

FIG. 8. Zonal averages of the temporal standard deviation of the daily sea level pressure (hPa). The data are the spatially unfiltered field (TOT) and the long (I), medium (II), and short (III) waves from the January GCM simulation. Plots are presented for (a) temporally unfiltered data, (b) bandpass, and (c) low-pass data.

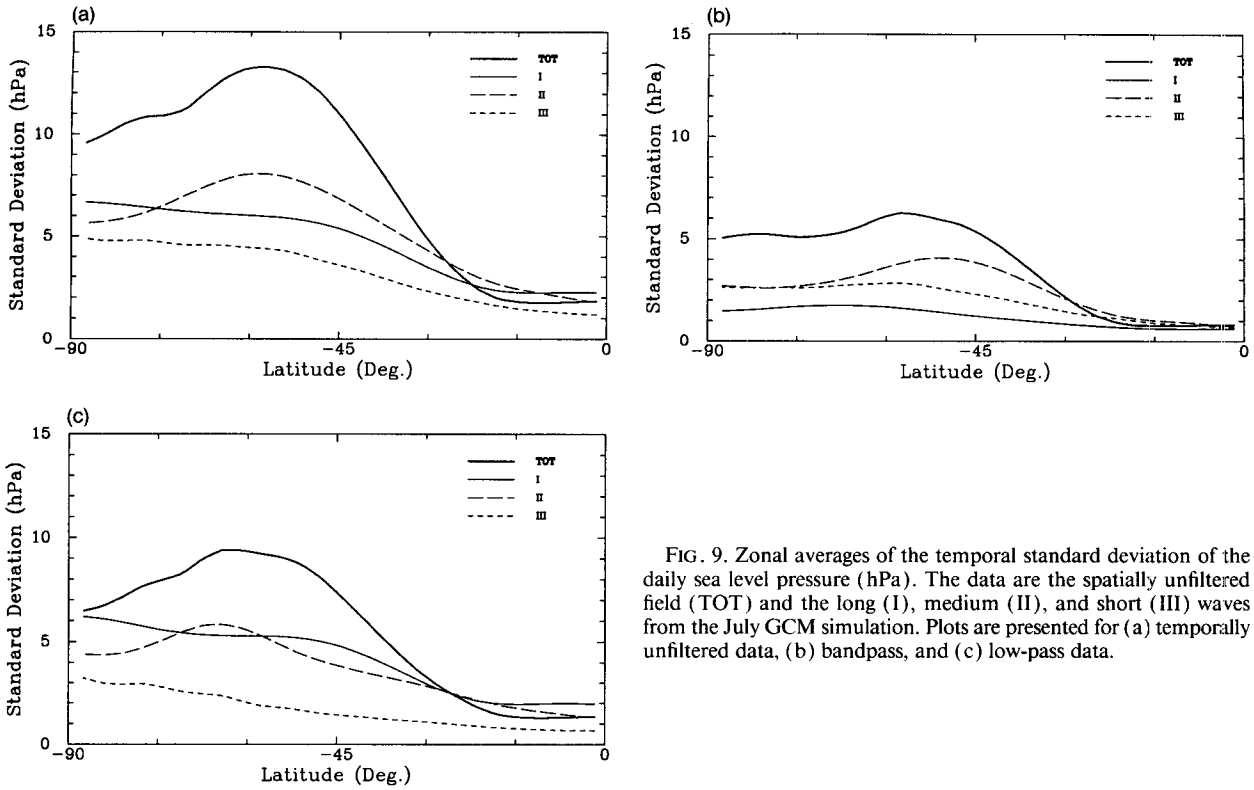

FIG. 9. Zonal averages of the temporal standard deviation of the daily sea level pressure (hPa). The data are the spatially unfiltered field (TOT) and the long (I), medium (II), and short (III) waves from the July GCM simulation. Plots are presented for (a) temporally unfiltered data, (b) bandpass, and (c) low-pass data.

Another, and perhaps more appropriate, method of defining storm tracks is in terms of a climatology of low pressure systems. We have described in Murray and Simmonds (1991a) a sophisticated automatic scheme for finding and tracking extratropical lows from digital analyses. The availability of such automatic schemes means that it is now no more difficult to obtain all the required statistics of low pressure systems than it is to calculate the temporal variation of some parameter. As in Murray and Simmonds (1991b), this scheme was applied to the same model-generated data used in this paper. Hence, a direct comparison of surface cyclone frequency and mean sea level variability is possible. Figure 2 in Murray and Simmonds (1991b) shows the January and July distribution of cyclones from the model climatology. Two of the strongest features in these months are the maxima at about 40° and 120°E near 60°S. Figure 10 shows the daily variability of the bandpass data for January and July. It is clear that the locations of the maxima of this quantity differ from those of cyclone density. The standard deviation maxima are situated some 30°–40° to the west and also farther north of those of cyclone density. This relative positioning appears consistent with Blackmon et al. (1977) who identified the high-pass filtered variability as associated with *developing* baroclinic disturbances. As to the position of the zonally averaged maxima, Murray and Simmonds (1991b) showed (their Fig. 7) the zonally averaged cyclone density maxima in both January and July to be at 62°S. In the present study, the maximum zonally averaged bandpass MSLP variability occurs farther to the north, at about 55°S in the two months (Figs. 8b and 9b). It is of interest to note that the maxima of the zonally average *low-pass* variability lie much closer to those of the cyclone density.

7. Concluding remarks

We have examined the contributions of several temporal and spatial modes to the total daily variability of mean sea level pressure over the Southern Hemisphere. This has been performed with 20 years of analyses generated by the Australian Bureau of Meteorology. The statistics generally display a deal of zonal symmetry, particularly in evidence during the summer period. The Antarctic and tropical regions are characterized by lower levels of variability, with a general enhancement evident throughout the midlatitudes. The core of largest variability is found to typically lie between 50° and 55°S, some 10° equatorward of the surface circumpolar trough. In January and July the percentage of the variance explained by the bandpass data is maximized between 30° and 60°S and assumes values of typically 25%. In general, the low-pass data account for more of the variance and tend to achieve its maxima in low and high latitudes.

Based on the NH definition of the storm tracks developed by Blackmon et al. (1977) and used in the SH by Trenberth (1981) and James and Anderson (1984),

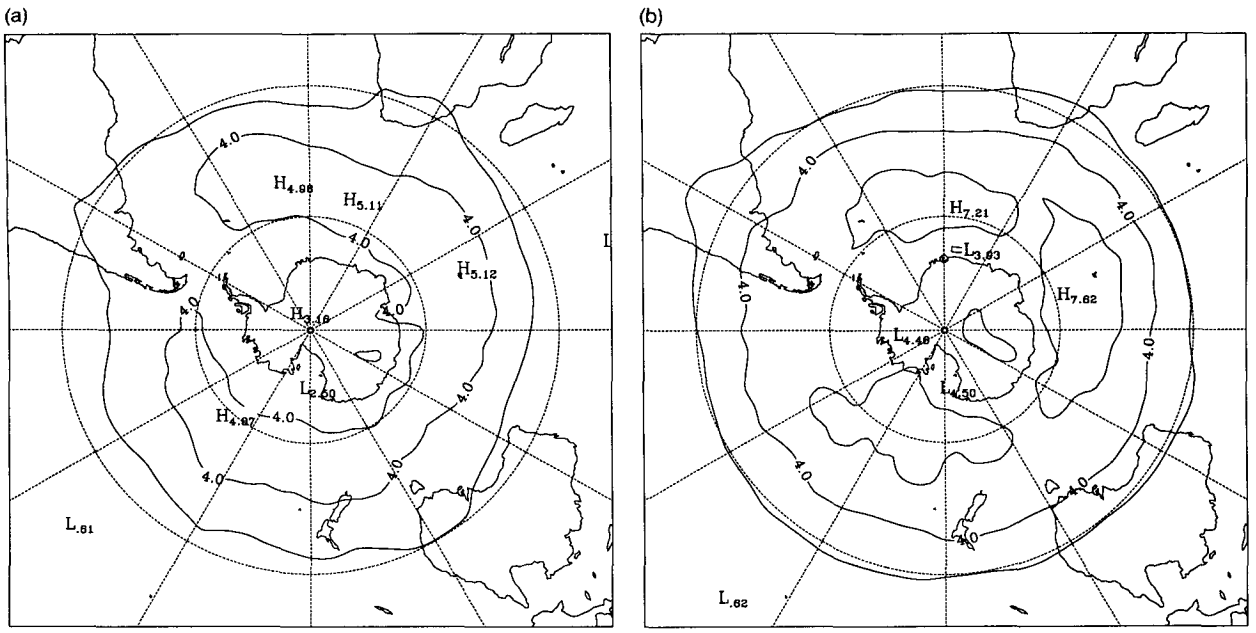

FIG. 10. Temporal standard deviation of the bandpassed daily sea level pressure in (a) January and (b) July from the GCM simulations. The contour interval is 2 hPa.

it would appear that there is a single storm track in the SH, this being located between 50° and 60°S and somewhat equatorward of the time–mean sub-Antarctic trough. We have found that the greatest contribution to the low-frequency field comes from the planetary-scale waves, particularly at higher latitudes. The synoptic and small-scale waves are generally found to be the chief contributors to the variability in the higher-frequency bandpass fields, particularly in the region of the hemispheric storm track.

These statistics have been compared with those derived from two perpetual-month climate simulations run with the Melbourne University GCM. In both the January and July simulations the model captured the essential features of the SH atmosphere with relatively small variability throughout the tropical and polar regions as well as a belt of enhanced variability of the simulated statistics through the midlatitudes. In general, the model's simulation of the high-frequency components of the variability is superior to that of the low-frequency components, with the storm track generated in the model simulation being similar to that inferred from the ASH statistics. In both simulations the model generated a spurious maximum in the low-frequency fields in the south Pacific upstream of the Drake Passage. Of note, the simulation of the time–mean distribution of the MSLP in this region is very good, indicating that a satisfactory simulation of the time–mean structure need not infer a skillful simulation of the transient behavior of the atmosphere.

In the low latitudes the model simulated erroneously low levels of variability. This underestimate suggests that through the tropics forced variations play a substantial role in inducing variability of the atmosphere, particularly at longer time scales; this has been commented on by a number of authors [e.g., Charney and Shukla (1981), Manabe and Hahn (1981), Lau (1981), Kushnir and Esbensen (1986) and Palmer (1987)]. Charney and Shukla (1981) speculated that the missing element in the model tropics is probably some boundary forcing, such as anomalies of the sea surface temperature or surface albedo. This is supported by Manabe and Hahn (1981) who concluded that the underestimate of the low-frequency components of the variability through the tropics in their study was due to the absence of long time-scale interactions between the atmosphere and ocean.

The simulated statistics generally displayed an increase in the role played by the small-scale features relative to that for the observational statistics. Whether the simulated statistics overemphasize the small wave participation relative to the real atmosphere is hard to judge, as the observational-analysis schemes used in the compilation of the observed statistics are generally biased against short waves. Comparison with independent analyses (e.g., those of the European Centre for Medium-Range Weather Forecasts and National Meteorological Center) may clarify this.

As has been pointed out by a number of authors, there is considerable ambiguity surrounding, or many definitions of, the term *storm tracks,* and it is not always clear how these relate to the classical understanding in terms of areas of high cyclone density. Making use of statistics produced by model simulations, we have been able to make a direct comparison of distribution of lows and of bandpassed variability. We find that the

maxima of both measures in the SH are reached at the high southern latitudes but that those of the bandpassed variability tend to be some 30°–40° of longitude to the west and 5°–7° latitude to the north of those of cyclone centers.

Acknowledgments. Some of this work was made possible by funding from the Australian Antarctic Science Advisory Committee.

REFERENCES

Blackmon, M. L., 1976: A climatological spectral study of the 500 mb geopotential height of the Northern Hemisphere. *J. Atmos. Sci.*, **33,** 1607–1623.

——, and N. Lau, 1980: Regional characteristics of the Northern Hemisphere wintertime circulation: A comparison of the simulation of a GFDL General Circulation Model with observations. *J. Atmos. Sci.*, **37,** 497–514.

——, J. M. Wallace, N. Lau, and S. L. Mullen, 1977: An observational study of the Northern Hemisphere wintertime circulation. *J. Atmos. Sci.*, 1040–1053.

Carleton, A. M., 1979: A synoptic climatology of satellite-observed extratropical cyclone activity for the Southern Hemisphere winter. *Arch. Meteor. Geophys. Bioklimatol.*, **27,** 265–279.

Charney, J. G., and J. Shukla, 1981: Predictability of monsoons. *Monsoon Dynamics*, Lighthill and Pearce, Eds. Cambridge University Press, 99–109.

Guymer, L. B., 1986: Procedures and Concepts used in Southern Hemisphere Analyses at WMC Melbourne. Preprints, *Second Int. Conf. on Southern Hemisphere Meteorology,* Amer. Meteor. Soc., 10–16.

Hoskins, B. J., and P. J. Valdes, 1990: On the existence of storm-tracks. *J. Atmos. Sci.*, **47,** 1854–1864.

——, I. N. James, and G. H. White, 1983: The shape, propagation, and mean flow interaction of large scale weather systems. *J. Atmos. Sci.*, **40,** 1595–1612.

James, I. N., and D. L. T. Anderson, 1984: Seasonal mean flow and distribution of large-scale weather systems in the Southern Hemisphere: The effects of moisture transports. *Quart. J. Roy. Meteor. Soc.*, **110,** 943–966.

Jenne, R. L., H. L. Crutcher, H. van Loon, and J. J. Taljaard, 1974: A selected climatology of the Southern Hemisphere: Computer methods and data availability. NCAR Tech. Note NCAR-TN/STR-92, 91 pp.

Kao, S. K., R. L. Jenne, and J. F. Sagendorf, 1970: The kinetic energy of large-scale atmospheric motion in wavenumber–frequency space. II: Mid-troposphere of the Southern Hemisphere. *J. Atmos. Sci.*, **27,** 1008–1020.

Karoly, D. J., and A. H. Oort, 1987: A comparison of Southern Hemisphere circulation statistics based on the GFDL and Australian analyses. *Mon. Wea. Rev.*, **115,** 2033–2059.

Kep, S. L., 1984: A climatology of cyclogenesis, cyclone tracks and cyclolysis in the Southern Hemisphere for the period 1972–81. [Available from University of Melbourne, Department of Meteorology, Pub. No. 25.]

Kushnir, Y., and S. K. Esbensen, 1986: Northern Hemisphere wintertime variability in a two-level general circulation model. Part I: Statistical characteristics of short and long time-scale disturbances. *J. Atmos. Sci.*, **43,** 2968–2983.

Lau, N.-C., 1981: A diagnostic study of recurrent meteorological anomalies appearing in a 15 year simulation with a GFDL general circulation model. *Mon. Wea. Rev.*, **109,** 2287–2311.

Le Marshall, J. F., G. A. M. Kelly, and D. J. Karoly, 1985: An atmospheric climatology of the Southern Hemisphere based on ten years of daily numerical analyses (1972–82). I: Overview. *Aust. Meteor. Mag.*, **33,** 65–85.

Manabe, S., and D. G. Hahn, 1981: Simulation of atmospheric variability. *Mon. Wea. Rev.*, **109,** 2260–2286.

Murray, R. J., and I. Simmonds, 1991a: A numerical scheme for tracking cyclone centres from digital data. Part I: Development and operation of the scheme. *Aust. Meteor. Mag.*, **39,** 155–166.

——, and I. Simmonds, 1991b: A numerical scheme for tracking cyclone centres from digital data. Part II: Application to January and July GCM simulations. *Aust. Meteor. Mag.*, **39,** 167–180.

Oort, A. H., 1983: Global atmospheric circulation statistics: 1958–1973. NOAA Prof. Paper No. 14. [Available from Govt. Printing Office, Washington, D.C.]

Palmer, T. N., 1987: Modelling low frequency variability of the atmosphere. *Atmospheric and Oceanic Variability,* H. Cattle, Ed., Royal Meteorological Society, 75–103.

Physick, W. L., 1981: Winter depression tracks and climatological jet stream in the Southern Hemisphere during the FGGE year. *Quart. J. Roy. Meteor. Soc.*, **107,** 883–898.

Simmonds, I., 1985: Analysis of the 'spinup' of a general circulation model. *J. Geophys. Res.*, **90,** 5637–5660.

——, G. Trigg, and R. Law, 1988: The climatology of the Melbourne University general circulation model. Pub. No. 31, 67 pp. [NTIS PB 88 227491.] [Available from Department of Meteorology, University of Melbourne]

——, P. Indusekharan, and R. J. Murray, 1990: A comparison of modelled and observed daily variability in the southern extratropics. *Aust. Meteor. Mag.*, **38,** 261–270.

Swanson, G. S., and K. E. Trenberth, 1981: Interannual variability in the Southern Hemisphere troposphere. *Mon. Wea. Rev.*, **109,** 1890–1897.

Taljaard, J. J., 1972: Synoptic meteorology of the Southern Hemisphere. *Meteor. Monogr.*, No. 13, Amer. Meteor. Soc., 139–213.

Trenberth, K. E., 1975: A quasi-biennial standing wave in the Southern Hemisphere and interrelations with sea surface temperature. *Quart. J. Roy. Meteor. Soc.*, **101,** 55–74.

——, 1981: Observed Southern Hemisphere eddy statistics at 500 mb: Frequency and spatial dependence. *J. Atmos. Sci.*, **38,** 2585–2605.

——, 1986: The signature of a blocking episode on the general circulation in the Southern Hemisphere. *J. Atmos. Sci.*, **43,** 2061–2069.

——, 1991: Storm tracks in the Southern Hemisphere. *J. Atmos. Sci.*, **48,** 2159–2178.

——, and K. C. Mo, 1985: Blocking in the Southern Hemisphere. *Mon. Wea. Rev.*, **113,** 3–21.

van Loon, H., 1956: Blocking in the Southern Hemisphere, Part I. *Notos,* **5,** 171–177.

——, 1965: A climatological study of the atmospheric circulation in the Southern Hemisphere during the IGY. Part I: 1 July 1957–31 March 1958. *J. Appl. Meteor.*, **4,** 479–491.

Wallace, J. M., G.-H. Lim, and M. L. Blackmon, 1988: Relationship between cyclone tracks, anticyclone tracks, and baroclinic waveguides. *J. Atmos. Sci.*, **45,** 439–462.